PROCEEDINGS B

rspb.royalsocietypublishing.org

Research

Cite this article: Eiting TP, Perot JB, Dumont ER. 2015 How much does nasal cavity morphology matter? Patterns and rates of olfactory airflow in phyllostomid bats. *Proc. R. Soc. B* **282**: 20142161.
http://dx.doi.org/10.1098/rspb.2014.2161

Received: 29 August 2014
Accepted: 18 November 2014

Subject Areas:
biomechanics, evolution

Keywords:
olfaction, ethmoturbinate, phyllostomid bats, computational fluid dynamics

Author for correspondence:
Thomas P. Eiting
e-mail: tom.eiting@utah.edu

†Present address: Department of Neurobiology and Anatomy, Brain Institute, University of Utah, Salt Lake City, UT 84132, USA.

THE ROYAL SOCIETY PUBLISHING

How much does nasal cavity morphology matter? Patterns and rates of olfactory airflow in phyllostomid bats

Thomas P. Eiting[1,†], J. Blair Perot[2] and Elizabeth R. Dumont[1,3]

[1]Graduate Program in Organismic and Evolutionary Biology, [2]Department of Mechanical and Industrial Engineering, and [3]Department of Biology, University of Massachusetts Amherst, Amherst, MA 01003, USA

The morphology of the nasal cavity in mammals with a good sense of smell includes features that are thought to improve olfactory airflow, such as a dorsal conduit that delivers odours quickly to the olfactory mucosa, an enlarged olfactory recess at the back of the airway, and a clear separation of the olfactory and respiratory regions of the nose. The link between these features and having a good sense of smell has been established by functional examinations of a handful of distantly related mammalian species. In this paper, we provide the first detailed examination of olfactory airflow in a group of closely related species that nevertheless vary in their sense of smell. We study six species of phyllostomid bats that have different airway morphologies and foraging ecologies, which have been linked to differences in olfactory ability or reliance. We hypothesize that differences in morphology correlate with differences in the patterns and rates of airflow, which in turn are consistent with dietary differences. To compare species, we make qualitative and quantitative comparisons of the patterns and rates of airflow through the olfactory region during both inhalation and exhalation across the six species. Contrary to our expectations, we find no clear differences among species in either the patterns of airflow through the airway or in rates of flow through the olfactory region. By and large, olfactory airflow seems to be conserved across species, suggesting that morphological differences appear to be driven by other mechanical demands on the snout, such as breathing and feeding. Olfactory ability may depend on other aspects of the system, such as the neurobiological processing of odours that work within the existing morphology imposed by other functional demands on the nasal cavity.

1. Introduction

Mammals that have a good sense of smell tend to have a suite of morphological features in their nasal cavity that are thought to be adaptations for improved olfactory ability. These features include a narrow, dorsal conduit for olfactory airflow, an enlarged cavity (the olfactory recess) at the back of the nasal airway and a clear separation of the olfactory region of the nose from the respiratory region [1–4]. All of these features impact the way air moves through the nasal cavity. The dorsal conduit delivers inhaled odorant-laden air relatively quickly to the back of the nose, where most of the olfactory epithelium is located [5]. We refer to this region as the 'ethmoturbinate region', because the ethmoturbinate bones, which are lined with olfactory mucosa, occupy this voluminous space. Once air reaches the ethmoturbinate region, it slows down dramatically, and it gradually courses ventrally and laterally, before exiting the nasal cavity at the back of the nose along with the respiratory air currents. Within the ethmoturbinate region is the olfactory recess, which is a blind pocket at the back of the nasal cavity. The principal function of the olfactory recess may be isolating the inhaled, odorant-laden air from exhaled respiratory air currents, which would otherwise be washed out by freshly inhaled odorants from the ethmoturbinate region [4–7].

The relationship between the morphology of the airway and olfactory airflow is based on detailed functional examinations of only a few species.

These studies have tended to focus on extremes in terms of both anatomy and olfactory ability: mammals with a large, restricted olfactory region and a well-developed sense of smell on the one hand (e.g. dogs [3,5]; rats [6–8]), and those with a small olfactory region and poorly developed sense of smell on the other (e.g. humans [9,10]). To date, no study has attempted to use a group of closely related species to more precisely link differences in their apparent reliance on olfaction with differences in airway morphology and patterns of airflow.

In this paper, we address this deficiency in our understanding by studying the anatomy and patterns of olfactory airflow in six species of ecologically diverse New World leaf-nosed bats (Family Phyllostomidae). These six species exhibit a broad range of dietary preferences that have been linked to differences in olfactory reliance. Our sample includes two basal insectivorous species (*Macrotus waterhousii* and *Mimon crenulatum*), two nectar-feeding bats (*Glossophaga soricina* and *Anoura geoffroyi*) and two frugivores (*Carollia perspicillata* and *Artibeus jamaicensis*; figure 1). Comparative neurobiological studies have consistently demonstrated that fruit- and nectar-feeders have larger olfactory brain structures compared with insectivores of the same brain and body size [11–13]. This has led some authors to suggest that diet is a major driving force in the evolution of differently sized olfactory regions (e.g. [12]). Behavioural studies support this suggestion. In fruit-eating bats like *Artibeus* and *Carollia*, olfactory cues are important in the detection and initial localization of food, and in distinguishing ripe from unripe fruit [14,15]. The nectar-feeders *Glossophaga* and *Anoura* also appear to rely on olfactory cues to detect food resources [16]; indeed, the 'chiropterophilly' floral syndrome includes characteristic odours [17–19]. However, these species generally switch to echolocation as they approach flowers [20]. Basal insectivores like *Mimon* and *Macrotus* probably do not use olfactory cues when foraging [15], although odours may be important in social interactions. For example, the closely related basal insectivore *Phyllostomus discolor* uses odour in mother–pup recognition [21].

The six species in our study also differ in the anatomy of their nasal cavity (figure 1). The rostra of fruit-eaters tend to be anteriorly–posteriorly compressed relative to those of basal insectivores, which allows them to generate relatively higher bite forces than longer-snouted species [22–24]. These species also tend to have ethmoturbinate spaces that are horizontally oriented (figure 1). Nectar-feeders, on the other extreme, tend to have elongated rostra, which extends the anterior region of their nasal cavities and vertically flattens the ethmoturbinate spaces (figure 1) [25]. The nasal cavities of insectivores tend to be intermediate between these two extremes (figure 1). Variation in the morphology of the nasal cavity among phyllostomids allows us to explicitly test the idea that morphological differences in the nasal cavity are associated with different patterns of olfactory airflow. Specifically, we predict that fruit- and nectar-feeders will have higher flow rates through the dorsal conduit compared with insect-feeders, to deliver odorants to the ethmoturbinate region more rapidly. We also predict that fruit- and nectar-feeders will have lower flow rates in the ethmoturbinate region compared with insect-eaters, because lower flow rates improve the efficiency of absorbing odorants [8,26]. Finally, we predict that during exhalation, more flow will bypass the olfactory recess and ethmoturbinate region in fruit- and nectar-feeders compared with insect-feeders. This would be beneficial because it would prevent recently inhaled odours from being washed out during exhalation, thereby increasing the amount of time odorant molecules are in contact with olfactory receptors lining the ethmoturbinate region.

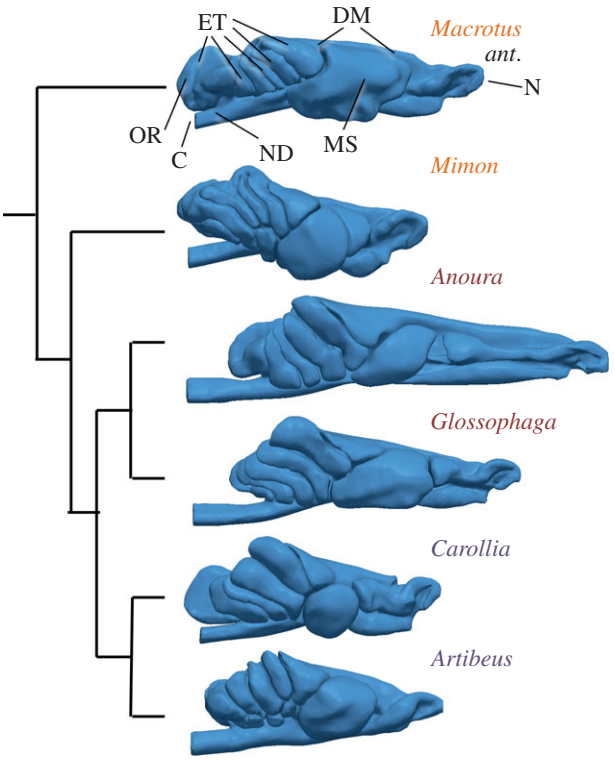

Figure 1. Phylogenetic relationships of the six species of bats used in our study, together with a lateral view of the right nasal airway for each species. Three-dimensional models are scaled to the same height, to give a sense of the dimensions of the airway regardless of size. Names of taxa are colour-coded to reflect diet: orange, insects; maroon, nectar; lavender, fruit. ant., anterior; C, choana; DM, dorsal meatus; ET, ethmoturbinate region; MS, maxillary sinus; N, naris; ND, nasopharyngeal duct; OR, olfactory recess. (Online version in colour.)

2. Material and methods

We constructed three-dimensional models of six species of bats from CT scans generated at the Harvard Center for Nanoscale Systems (table 1). For each species, we constructed a 3D stereolithography (STL) file from the CT scans as follows (see [4] for additional details). First, an image stack was brought into Mimics v. 16.0 (Materialise, Leuven, Belgium). Once imported, we digitally isolated the airway by using a combination of thresholding and individual editing of slices, sometimes with the aid of comparisons to histological preparations (see [32], for details of the histological procedure). We imported the STL into Geomagic Studio v. 12.0 (3D Systems, Rock Hill, SC), which we used to further refine the model because the fluid dynamics software requires a smooth mesh. At this step, we artificially elongated the nasopharyngeal meatus (ventral-most posterior channel of the nasal cavity) to ensure fully developed flow during exhalation in our region of interest (i.e. the ethmoturbinate region). The artificially elongated segment varied in length in each model, according to the equation

$$L_e = 0.06Re \times D, \tag{2.1}$$

where L_e is the entrance length (i.e. the length of the elongated segment, in mm), Re is the Reynolds number (approx. 20 for each model) and D is the diameter of the nasopharyngeal meatus (in mm), which approximates the geometry of a pipe. For our models, L_e varied from 0.6 mm in *Mimon crenulatum* to 2.4 mm in *Artibeus jamaicensis*.

Table 1. Details of the specimens, scanning and model parameters used in this study. AMNH, American Museum of Natural History.

species	AMNH no.	pixel size (μm)	no. elements in final model	inhalation velocity ($m\,s^{-1}$)	exhalation velocity ($m\,s^{-1}$)	average body mass (g)	diet [27]
Macrotus waterhousii	275472	19.9	622 448	1.04	3.0×10^{-1}	16 [28]	I
Mimon crenulatum	267888	18.2	636 550	9.02×10^{-1}	3.54×10^{-1}	14.5 [23]	I
Anoura geoffroyi	199538	24.3	616 119	6.5×10^{-1}	2.25×10^{-1}	12.8 [29]	N
Glossophaga soricina	260965	19	622 685	9.65×10^{-1}	1.75×10^{-1}	10 [30]	N
Carollia perspicillata	261433	24.3	623 269	1.17	3.0×10^{-1}	18.5 [31]	F
Artibeus jamaicensis	267998	26.7	633 591	1.64	2.75×10^{-1}	48 [23]	F

Once the STL file was sufficiently refined, we re-imported it back into Mimics, where we created a solid model of the airway. For each species, the solid model comprises approximately 625 000 four-noded tetrahedral elements (table 1). We performed a grid-refinement study by examining patterns and rates of flow in models with twice and four times as many bricks. We did not find notable differences in either parameter, corroborating our previous work [4], and indicating that the approximately 625 000-tetrahedra models were sufficient for this study.

All six solid models were exported from Mimics as MSH files, which were compatible with our computational fluid dynamics (CFD) software, OpenFOAM v. 1.6-ext (www.openfoam.org). We used OpenFOAM to solve steady-state solutions of inhalation and exhalation. For each simulation, we applied a constant inflow velocity across the inlet (i.e. the naris during inhalation, and the choana during exhalation), a zero velocity gradient and constant pressure boundary at the outlet (i.e. the choana during inhalation, and the naris during exhalation). We scaled the volumetric flow rate in each species by applying the allometric equation (from [5])

$$Q_{\text{peak}} = 1.43M^{1.04\pm0.03}, \tag{2.2}$$

where Q_{peak} is peak inspiratory flow rate (i.e. during sniffing) and M is the body mass (in grams). Each value of Q_{peak} was converted to flow velocity by dividing it by the area of the inlet normal to the direction of flow. The final velocities applied during both inhalation and exhalation for all six models can be seen in table 1. We performed a sensitivity analysis on flow rate by calculating volumetric flow rate according to the error in the exponent in equation (2.2) (i.e. we calculated a high and low value of Q_{peak} by multiplying M by 1.07 and 1.01). The results were not appreciably different, so we only show the results from using an exponent of 1.04. All simulations were performed using the 'icofoam' solver in OpenFOAM. Icofoam is a second-order accurate finite volume method that solves the laminar, incompressible, constant-velocity Navier–Stokes equations. We used the kinematic viscosity of air at 30°C, which is $1.6 \times 10^{-5}\,m^2\,s^{-1}$. Though the velocity of air moving through the nasal passages is in fact time-varying, we assumed steady-state flow to match most previous work on the subject (e.g. [4–10]) and because good agreement exists between patterns of flow between steady and unsteady regimes [33].

To address our hypotheses, we performed both qualitative and quantitative analyses of patterns and rates of flow using the visualization software Paraview v. 4.1.0 (Kitware, Clifton Park, New York, NY). We compared patterns of flow by observing the location of streamlines (i.e. lines of flow tangential to the direction of flow) for each simulation. We visualized streamlines by colouring them according to magnitude of the flow velocity. It was necessary to scale the streamline colours to a maximum of $0.3\,m\,s^{-1}$ to achieve a dispersion of colours. In reality, the maximum flow rates (which occurred near the naris and the choana) were roughly an order of magnitude higher than the upper colour bound.

We also compared inhalation flow velocities in the ethmoturbinate region. First, we identified an area within each model that closely approximated the ethmoturbinate region. We then selected this region as follows: we selected the first anterior–posterior slice in which we saw a lateral expansion of the nasal airway, and then expanded our selection to include the folded regions between ethmoturbinates. We then used the pattern of streamlines during inhalation to remove portions of the selected area that were predicted to transmit only respiratory flow. Once the ethmoturbinate region was selected for each species, we calculated average flow velocity in the region by integrating flow velocity in each brick over the selected volume. For each species, we repeated the process of selecting the ethmoturbinate region and calculating average flow velocity a minimum of three times, to assure that our selection procedures and calculations were repeatable. We found variation in flow velocity to be under about 10%, so we report values rounded to the nearest order of magnitude.

It is important to point out that no statistical analyses are possible in this study, because there is no 'sample size' in the traditional sense. Each species is represented by a model of only one specimen, so there is no intraspecies variability to report. Therefore, we have tried to not over-interpret quantitative values produced from our analyses, and we do not present any statistical differences between species, or other similar quantities.

3. Results

Patterns of flow during inhalation in all species show that most air passes ventrally through the nasal airway, en route to the nasopharyngeal duct (figure 2). Air that enters the naris dorsally tends to flow via a dorsal conduit to the rear of the nasal cavity (i.e. the ethmoturbinate region), where most of the olfactory epithelium is located. Compared with the ethmoturbinate region, flow along the dorsal conduit tends to be faster. Once air from the dorsal conduit reaches the ethmoturbinate region, it slows down substantially. As it does so, it migrates ventrally and laterally (figure 2), before passing over the transverse lamina and then exiting the airway at the choana, along with the rest of the non-olfactory inhaled air.

We also calculated average flow velocity over the volume of the nasal airway that encompassed the ethmoturbinate region. Calculated flow velocities in this region were in the range of 1.03×10^{-2}–$1.53 \times 10^{-2}\,m\,s^{-1}$ (figure 3*a*). There are no significant differences among the dietary groups, though nectar-feeders do seem to have slightly higher flow rates in the ethmoturbinate region compared with fruit-eaters. We also standardized flow rates by dividing flow speeds in the ethmoturbinate region by the inhaled flow speed that was applied at the inlet (i.e. naris). Doing so provided us with a velocity-independent metric for how much the air

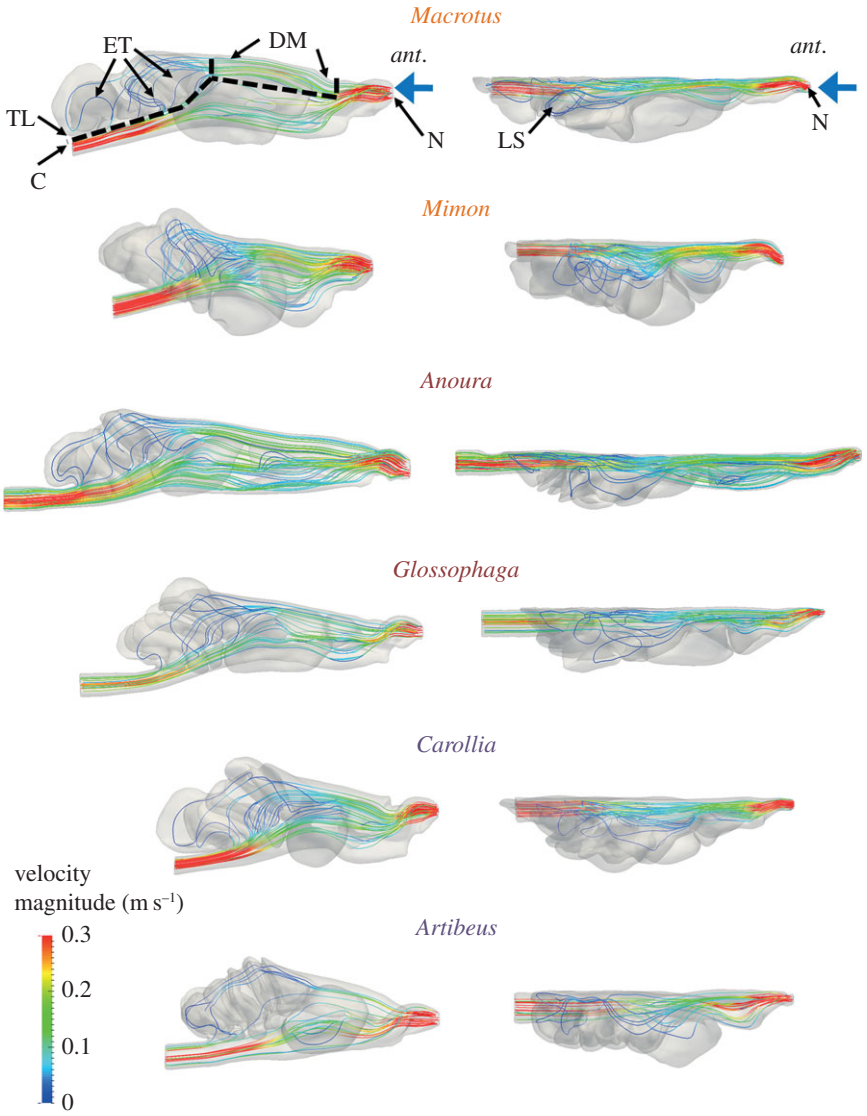

Figure 2. Lateral (left) and dorsal (right) views of right nasal cavity of six species of bats, showing patterns and rates of airflow during inhalation. Flow paths are shown as streamlines, and rates of flow are shown in colour. Inhaled air was forced through the naris (N) in the direction of the large blue arrow. Streamlines are scaled to the same velocity magnitude in all six models. Dashed lines separate regions of interest. In the lateral views, note in general how a dorsal meatus (DM) of relatively high flow speeds delivers air to the more posterior ethmoturbinate region (ET), where flow speeds tend to be lower. After passing through the ethmoturbinate region, flow passes over the transverse lamina (TL) and exits at the choana (C). In the dorsal views, note the lateral streamline (LS) that migrates ventrally and laterally before exiting the airway (ant., anterior). (Online version in colour.)

passing through the ethmoturbinate region slows down compared with inhaled flow speeds. Figure 3*b* shows that the flow speed in the ethmoturbinate region is approximately 1% of the flow speed at the naris. Nectar-feeders seem to perform slightly more poorly as judged from this metric, though only by a factor of about four at most (2.4% in *Anoura geoffroyi* versus 0.6% in *Artibeus jamaicensis*).

During exhalation in all species, most air again bypasses the ethmoturbinate region on its way through the main airway (figure 4), although some flow does pass through the ethmoturbinate region before exiting at the naris. As during inhalation, exhaled air that passes through the ethmoturbinate region tends to be moving much more slowly than the air that passes through other parts of the nasal airway.

4. Discussion

Despite their significant morphological differences, all six species showed similar patterns and rates of airflow during inhalation (figure 2). They all have a dorsal conduit through which inhaled air moves before reaching the convoluted ethmoturbinate region, where flow speeds decrease substantially. We do not find notable variation across species in the rates of flow through this dorsal conduit. From here, air tends to enter the ethmoturbinate region medially (figure 2). Once within the ethmoturbinate complex, air passes laterally and ventrally, before finally meeting up with the respiratory flow and exiting via the choana. The quantitative results supplement these qualitative findings in important ways. Rates of flow in the ethmoturbinate region do not vary substantially among the six species, varying only by a factor of 1.5. Even though the flow speed in this region is highest in the nectar-feeding species and lowest in the fruit-eaters, it is not clear whether this variation is meaningful. The flow speeds we predict in the ethmoturbinate region are within the range seen in rodents [6], raising the possibility that an optimum or range of optima may exist for flow speeds that successfully deliver odorants to olfactory receptors. To more fully address this idea, performing analyses of odorant deposition during transient

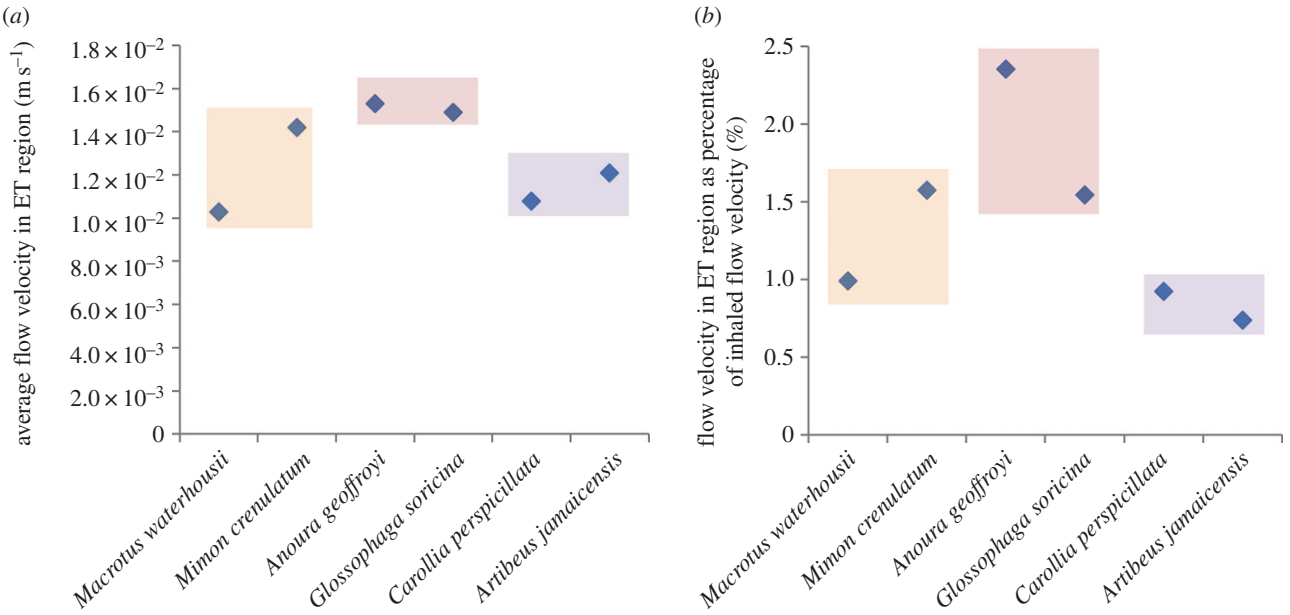

Figure 3. (*a*) Average flow velocity in the ethmoturbinate region during inhalation across six species of bats. (*b*) Relative flow velocity in the ethmoturbinate region (i.e. ethmoturbinate velocity divided by velocity at the inlet) across six species of bats, expressed as a percentage. In both plots, species are enclosed within a box that is colour-coded according to diet as in figure 1. (Online version in colour.)

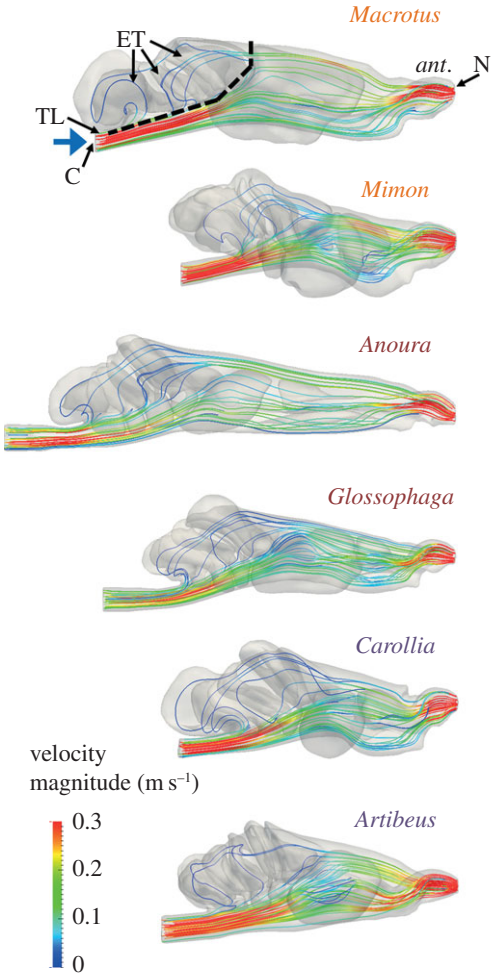

Figure 4. Lateral view of the right nasal cavity showing patterns and rates of airflow during exhalation. The paths of flow are indicated by streamlines, and rates of flow are indicated by colour. Exhaled air was forced through the nasopharyngeal duct at the location of the large blue arrows. Streamlines are scaled to the same velocity magnitude in all six models. Note in general how streamlines pass through the olfactory/ethmoturbinate region (ET), suggesting that this region is not isolated from expiratory airflow. Labels as in figure 2. (Online version in colour.)

(i.e. time-varying) flow would be beneficial. Unfortunately, such an analysis is not feasible given current modelling techniques and computational power.

The patterns of airflow during inhalation seen across all six bat species are very similar to those observed in dogs and rats [5,7], perhaps suggesting common functional demands for olfactory airflow and performance across a broad array of mammals. During exhalation, however, bats differ from rodents and dogs, in which all exhaled air is predicted to bypass the olfactory recess. Rather, in all six species of bats, our models predict that some air passes through the olfactory recess before being finally exhaled. This is especially surprising in species like *Mimon crenulatum* and *Carollia perspicillata*, which have fairly large olfactory recesses that contain as much as a third of all of the olfactory epithelium [32]. The implication of this finding is that, rather than sequestering recently inhaled air from exhalation, the primary functions of the olfactory recess in these phyllostomid bats may be to expand the surface area available for the olfactory epithelium and slow down inhaled air to improve odorant absorption across this epithelium. Some computational support for this idea was found by Eiting *et al*. [4], who showed in an experimental modelling study that, all else being equal, a larger olfactory recess produces lower rates of flow through this region during exhalation.

The suggestion that the olfactory recess functions to reduce airflow speed is tentative because the effect of low flow speed on odorant transport and deposition may be context-dependent. Studies have fairly consistently shown that higher flow rates produce greater total odorant absorption by the olfactory epithelium; faster flow means more odorant particles are absorbed per unit time [8,34]. This could be beneficial to species that are trying to detect environmental odorants in low concentrations. For example, the bat *Carollia perspicillata* is known to increase its sniffing frequency (and thus its flow rate) when sampling odorants just above threshold concentration [14]. A similar result is also found in the rat [35]. However, higher flow rates also produce less *relative* odorant absorption. In other words, as flow rate

increases, a smaller fraction of suspended odorant molecules is absorbed by the olfactory epithelium. This might not be a problem if an animal is trying to detect strong odours, but if the goal is to maximize discrimination among odorants, or if odorants are present at very low densities or in a finite quantity, then improving absorption efficiency (i.e. relative odorant flux) via lower flow rates may be important.

Many studies have shown that odorants with different solubilities are deposited along different regions of the olfactory mucosa [8,34–37]. This separation of odorants along the path of flow matches, at least to a first approximation, the location of the relevant olfactory receptors within the olfactory epithelium [38,39]. Performing transient analyses of odorant deposition would be an informative way to examine the generality of the hypothesized link between the 'inherent' pattern of olfactory gene expression and the 'imposed' pattern of odorant delivery by inhaled air (terminology after [37]). Such analyses would also allow us to generate hypotheses about the location and relative abundance of particular types of olfactory receptors expressed throughout the epithelium, and the possible link with ecologically relevant odours.

Despite notable variation in the shapes of the nasal passages in phyllostomid bats, the patterns and rates of airflow across the clade appear very similar (figures 2–4). These results suggest that olfactory airflow and its relationship to the morphology of the nasal airways may be a case of many-to-one mapping, in which functional similarity can occur despite morphological variability [40,41]. In the four-bar linkage system of fish jaws, for instance, functional equivalence in kinematic transmission can be produced through a variety of morphologically distinct phenotypes [42]. If the nasal cavity is yet another example of this phenomenon, then the morphology of the airway may not be under strong selection pressure to change with shifting olfactory functional demands. Stated another way, there may be strong selection for olfactory function, such as reducing flow rates and recirculating airflow in the olfactory recess, but this functionality can be achieved through many different forms. Demands on the olfactory system may be met more easily by changing aspects of the neurobiological system, such as the number of glomeruli or mitral cells in the olfactory bulb [43]. Variation in the shape of the nasal cavity (and the skull more generally) may be tied more to mechanical aspects of the rostrum, such as breathing and feeding, that more clearly depend upon shape for function. It could also be the case that the relatively invariant patterns and rates of flow that we see are the result of phylogenetic effects. In this scenario, ancestral phyllostomids may have had a morphology already well suited for olfaction, perhaps because of the emphasis that bats (and mammals in general) place on olfaction to mediate communication [44]. Using olfaction to aid in foraging may have been a relatively 'easy addition' to species that already rely on olfaction for other functions. Disentangling these various explanations would be an exciting avenue for future research, which may lead to new understanding of the relationship between form and function.

Data accessibility. Computed tomography scans and solid models of the nasal cavities for each species (suitable for running CFD simulations) have been made available on Dryad (doi:10.5061/dryad.2171f) and on the Biomesh repository (www.biomesh.org).

Acknowledgements. We thank Nancy Simmons and Eileen Westwig, American Museum of Natural History, for access to the bat specimens used in this study. Nancy Forger and Geert DeVries generously provided access to the laboratory equipment used in the histological sampling. Mike Martell, Chris Zusi and Yang Song provided assistance with the CFD techniques. We thank Tim Smith, members of the Dumont Lab, the Behavior and Morphology group at the University of Massachusetts and two anonymous reviewers for comments that helped improve the manuscript.

Funding statement. This work was supported by a National Science Foundation (NSF) Doctoral Dissertation Improvement Grant (DEB-1110641 to T.P.E.) and the NSF Division of Biological Infrastructure (DBI-0743460 to E.R.D.). This work was performed in part at the Center for Nanoscale Systems (CNS) of Harvard University, a member of the National Nanotechnology Infrastructure Network (NNIN), which is supported by the National Science Foundation (ECS-0335765).

References

1. Negus V. 1958 *The comparative anatomy and physiology of the nose and paranasal sinuses*. Edinburgh, UK: Livingstone.
2. Moore WJ. 1981 *The mammalian skull*. Cambridge, UK: Cambridge University Press.
3. Craven BA, Neuberger T, Paterson EG, Webb AG, Josephson EM, Morrison EE, Settles GS. 2007 Reconstruction and morphometric analysis of the nasal airway of the dog (*Canis familiaris*) and implications regarding olfactory airflow. *Anat. Rec.* **290**, 1325–1340. (doi:10.1002/ar.20592)
4. Eiting TP, Smith TD, Perot JB, Dumont ER. 2014 The role of the olfactory recess in olfactory airflow. *J. Exp. Biol.* **217**, 1799–1803. (doi:10.1242/jeb.097402)
5. Craven BA, Paterson EG, Settles GS. 2010 The fluid dynamics of canine olfaction: unique nasal airflow patterns as an explanation of macrosmia. *J. R. Soc. Interface* **7**, 933–943. (doi:10.1098/rsif.2009.0490)
6. Zhao K, Dalton P, Yang GC, Scherer PW. 2006 Numerical modeling of turbulent and laminar airflow and odorant transport during sniffing in the human and rat nose. *Chem. Senses* **31**, 107–118. (doi:10.1093/chemse/bjj008)
7. Yang GC, Scherer PW, Mozell MM. 2007 Modeling inspiratory and expiratory steady-state velocity fields in the sprague-dawley rat nasal cavity. *Chem. Senses* **32**, 215–223. (doi:10.1093/chemse/bjl047)
8. Yang GC, Scherer PW, Zhao K, Mozell MM. 2007 Numerical modeling of odorant uptake in the rat nasal cavity. *Chem. Senses* **32**, 273–284. (doi:10.1093/chemse/bjl056)
9. Keyhani K, Scherer PW, Mozell MM. 1995 Numerical simulation of airflow in the human nasal cavity. *J. Biomech. Eng.* **117**, 429–441. (doi:10.1115/1.2794204)
10. Keyhani K, Scherer PW, Mozell MM. 1997 A numerical model of nasal odorant transport for the analysis of human olfaction. *J. Theor. Biol.* **186**, 279–301. (doi:10.1006/jtbi.1996.0347)
11. Barton RA, Purvis A, Harvey PH. 1995 Evolutionary radiation of visual and olfactory brain systems in primates, bats and insectivores. *Phil. Trans. R. Soc. Lond. B* **348**, 381–392. (doi:10.1098/rstb.1995.0076)
12. Hutcheon JM, Kirsch JAW, Garland Jr T. 2002 A comparative analysis of brain size in relation to foraging ecology and phylogeny in the Chiroptera. *Brain Behav. Evol.* **60**, 165–180. (doi:10.1159/000065938)
13. Safi K, Dechmann DKN. 2005 Adaptation of brain regions to habitat complexity: a comparative analysis in bats (Chiroptera). *Proc. R. Soc. B* **272**, 179–186. (doi:10.1098/rspb.2004.2924)
14. Laska M. 1990 Olfactory discrimination ability in short-tailed fruit bat, *Carollia perspicillata* (Chiroptera: Phyllostomatidae). *J. Chem. Ecol.* **16**, 3291–3299. (doi:10.1007/BF00982099)
15. Altringham J, Fenton M. 2003 Sensory ecology and communication in the Chiroptera. In *Bat ecology* (eds T Kunz, MB Fenton), pp. 90–127. Chicago, IL: University of Chicago Press.
16. von Helversen O, Winkler L, Bestmann HJ. 2000 Sulphur-containing 'perfumes' attract flower-visiting

bats. *J. Comp. Physiol. A* **186**, 143–153. (doi:10.1007/s003590050014)

17. Knudsen JT, Tollsten L. 1995 Floral scent in bat-pollinated plants: a case of convergent evolution. *Bot. J. Linn. Soc.* **119**, 45–57. (doi:10.1111/j.1095-8339.1995.tb00728.x)
18. von Helversen O, Voigt CC. 2002 Glossophagine bat pollination in *Helicteres baruensis* (Sterculiaceae). *Ecotropica* **8**, 23–30.
19. Pettersson S, Ervik F, Knudsen JT. 2004 Floral scent of bat-pollinated species: West Africa vs. the New World. *Biol. J. Linn. Soc.* **82**, 161–168. (doi:10.1111/j.1095-8312.2004.00317.x)
20. von Helversen D, von Helversen O. 2003 Object recognition by echolocation: a nectar-feeding bat exploiting the flowers of a rain forest vine. *J. Comp. Physiol. A* **189**, 327–336.
21. Bloss J. 1999 Olfaction and the use of chemical signals in bats. *Acta Chiropterol.* **1**, 31–45.
22. Freeman PW. 1988 Frugivorous and animalivorous bats (Microchiroptera): dental and cranial adaptations. *Biol. J. Linn. Soc.* **33**, 249–272. (doi:10.1111/j.1095-8312.1988.tb00811.x)
23. Santana SE, Dumont ER. 2009 Connecting behaviour and performance: the evolution of biting behaviour and bite performance in bats. *J. Evol. Biol.* **22**, 2131–2145. (doi:10.1111/j.1420-9101.2009.01827.x)
24. Dumont ER, Dávalos LM, Goldberg A, Santana SE, Rex K, Voigt CC. 2012 Morphological innovation, diversification and invasion of a new adaptive zone. *Proc. R. Soc. B* **279**, 1797–1805. (doi:10.1098/rspb.2011.2005)
25. Freeman PW. 2000 Macroevolution in Microchiroptera: recoupling morphology and ecology with phylogeny. *Evol. Ecol. Res.* **2**, 317–335.
26. Mozell MM, Sheehe PR, Swieck S, Kurtz DB, Hornung DE. 1984 A parametric study of the stimulation variables affecting the magnitude of the olfactory nerve response. *J. Gen. Physiol.* **83**, 233–267. (doi:10.1085/jgp.83.2.233)
27. Ferrarezzi H, Gimenez E. 1996 Systematic patterns and the evolution of feeding habits in Chiroptera (Archonta: Mammalia). *J. Comp. Biol.* **1**, 75–94.
28. Hosken DJ. 1997 Sperm competition in bats. *Proc. R. Soc. Lond. B* **264**, 385–392. (doi:10.1098/rspb.1997.0055)
29. Ortega J, Alarcón DI. 2008 *Anoura geoffroyi* (Chiroptera: Phyllostomidae). *Mamm. Species* **818**, 1–7. (doi:10.1644/818.1)
30. Alvarez J, Willig MR, Jones Jr JK, Webster WD. 1991 *Glossophaga soricina. Mamm. Species* **379**, 1–7. (doi:10.2307/3504146)
31. Cloutier D, Thomas DW. 1992 *Carollia perspicillata. Mamm. Species* **417**, 1–9.
32. Eiting TP, Smith TD, Dumont ER. 2014 Olfactory epithelium in the olfactory recess: a case study in new world leaf-nosed bats. *Anat. Rec.* **297**, 2105–2112. (doi:10.1002/ar.23030)
33. Jiang J, Zhao K. 2010 Airflow and nanoparticle deposition in rat nose under various breathing and sniffing conditions—a computational evaluation of the unsteady and turbulent effect. *J. Aerosol Sci.* **41**, 1030–1043. (doi:10.1016/j.jaerosci.2010.06.005)
34. Lawson MJ, Craven BA, Paterson EG, Settles GS. 2012 A computational study of odorant transport and deposition in the canine nasal cavity: implications for olfaction. *Chem. Senses* **37**, 553–566. (doi:10.1093/chemse/bjs039)
35. Youngentob SL, Mozell MM, Sheehe PR, Hornung DE. 1987 A quantitative analysis of sniffing strategies in rats performing odor detection tasks. *Physiol. Behav.* **41**, 59–69. (doi:10.1016/0031-9384(87)90131-4)
36. Mozell MM. 1966 The spatiotemporal analysis of odorants at the level of the olfactory receptor sheet. *J. Gen. Physiol.* **50**, 25–41. (doi:10.1085/jgp.50.1.25)
37. Moulton DG. 1976 Spatial patterning of response to odors in the peripheral olfactory system. *Physiol. Rev.* **56**, 578–593.
38. Ressler KJ, Sullivan SL, Buck LB. 1993 A zonal organization of odorant receptor gene expression in the olfactory epithelium. *Cell* **73**, 597–609. (doi:10.1016/0092-8674(93)90145-G)
39. Schoenfeld TA, Cleland TA. 2006 Anatomical contributions to odorant sampling and representation in rodents: zoning in on sniffing behavior. *Chem. Senses* **31**, 131–144. (doi:10.1093/chemse/bjj015)
40. Alfaro ME, Bolnick DI, Wainwright PC. 2004 Evolutionary dynamics of complex biomechanical systems: an example using the four-bar mechanism. *Evolution* **58**, 495–503. (doi:10.1111/j.0014-3820.2004.tb01673.x)
41. Wainwright PC, Alfaro ME, Bolnick DI, Hulsey CD. 2005 Many-to-one mapping of form to function: a general principle in organismal design? *Integr. Comp. Biol.* **45**, 256–262. (doi:10.1093/icb/45.2.256)
42. Hulsey CD, Wainwright PC. 2002 Projecting mechanics into morphospace: disparity in the feeding system of labrid fishes. *Proc. R. Soc. Lond. B* **269**, 317–326. (doi:10.1098/rspb.2001.1874)
43. Royet J-P, Distel H, Hudson R, Gervais R. 1998 A re-estimation of the number of glomeruli and mitral cells in the olfactory bulb of rabbit. *Brain Res.* **788**, 35–42. (doi:10.1016/S0006-8993(97)01504-7)
44. Anisko JJ. 1976 Communication by chemical signals in Canidae. In *Mammalian olfaction, reproductive processes and behavior* (ed. RL Doty), pp. 283–293. New York, NY: Academic Press.